Top quark polarization as a probe of models with extra gauge bosons

Edmond L. Berger, Qing-Hong Cao, Chuan-Ren Chen, and Hao Zhang

Top Quark Polarization As A Probe of Models
with Extra Gauge Bosons

Edmond L. Berger,[1, *] Qing-Hong Cao,[1, 2, †] Chuan-Ren Chen,[3, ‡] and Hao Zhang[4, §]

[1]*High Energy Physics Division, Argonne National Laboratory, Argonne, IL 60439, U.S.A*

[2]*Enrico Fermi Institute, University of Chicago, Chicago, Illinois 60637, U.S.A.*

[3]*Institute for Physics and Mathematics of the Universe,*

University of Tokyo, Chiba 277-8568, Japan

[4]*Department of Physics and State Key Laboratory of Nuclear Physics and Technology,*

Peking University, Beijing 100871, China

Abstract

New heavy gauge bosons exist in many models of new physics beyond the standard model of particle physics. Discovery of these W' and Z' resonances and the establishment of their spins, couplings, and other quantum numbers would shed light on the gauge structure of the new physics. The measurement of the polarization of the SM fermions from the gauge boson decays would decipher the handedness of the coupling of the new states, an important relic of the primordial new physics symmetry. Since the top quark decays promptly, its decay preserves spin information. We show how decays of new gauge bosons into third generation fermions ($W' \to tb$, $Z' \to t\bar{t}$) can be used to determine the handedness of the couplings of the new states and to discriminate among various new physics models.

---

[*]Electronic address: `berger@anl.gov`

[†]Electronic address: `caoq@hep.anl.gov`

[‡]Electronic address: `chuan-ren.chen@ipmu.jp`

[§]Electronic address: `haozhang.pku@pku.edu.cn`

I. INTRODUCTION

One of the missions of the Large Hadron Collider (LHC) is to piece together some of nature's original symmetries. The search for these symmetries is a part of the ultimate quest to unify all of the particles and forces within a grand unified theory that exhibits overarching gauge symmetries. Theoretical clues to the original state of symmetry may be present in conserved or nearly conserved quantities in nature today. As remnants of symmetry breaking, extra gauge bosons exist in many models of new physics (NP) that go beyond the standard model (SM). The discovery of new neutral and charged gauge bosons and the establishment of their quantum numbers would shed light on the gauge structure of NP [1–17].

One salient property of new gauge bosons is the handedness of their couplings to SM fermions, whether dominantly left-handed as the SM W and Z vector bosons or possibly with large right-handed couplings. In this paper we focus on new color-singlet W' and Z' production at the LHC and their decays into the third generation SM fermions t, b. We explore quantitatively the measurement of the chirality of the couplings of the new gauge bosons from the polarization of the top quarks in their decays.[1] The top quark is the only "bare" quark whose spin information can be measured from its decay products since the decay proceeds promptly via the weak interaction. Among the top quark decay products, the charged lepton from $t \to b\ell\nu$ is the best analyzer of the top quark spin. In the helicity basis, the polarization of the top quark can be determined from the distribution in θ_ℓ, the angle of the lepton in the rest frame of top quark relative to the top quark direction of motion in the overall center-of-mass (cm) frame. The angular correlation of the lepton ℓ^+ is $\frac{1}{2}(1 \pm \cos\theta_\ell)$, with the $(+)$ choice for right-handed and $(-)$ for left-handed top-quarks [20, 21].

In addition to the matter of handedness of couplings, there are other reasons to search for the Z'/W' in $t\bar{t}$ and tb events. One is that searches in the leptonic decay modes would fail in the so-called leptophobic models because the Z' and W' bosons in these models do not couple to leptons. Searches in dijet invariant mass distributions are valuable but cannot determine whether a dijet resonance is a Z' or W' boson because the jet charge is not measurable. In such cases, the third generation quarks are necessary for charge determinations of the heavy

---

[1] The top quark polarization can also be used to probe new gauge bosons and scalars in exotic color representation such as sextet and anti-triplet; see Ref. [18, 19] for details.

resonances; for example, the Z' bosons decay into $t\bar{t}$ and $b\bar{b}$ pairs and the W' bosons into $t\bar{b}$ and $\bar{t}b$ pairs.

In Sec. II, we describe models of new physics that contain extra gauge bosons and show how patterns of symmetry breaking are manifest in the handedness of the couplings of the new gauge bosons to SM fermions. We illustrate a few of the NP models from the current literature. This section also includes a summary of the existing constraints on masses and couplings of new gauge bosons. In Sec. III, we present W' and Z' production cross sections at the LHC, both the inclusive rates and the rates of interest to us with all branching fractions included. The collider signatures we study are $\ell^{+}\not{E}_{T}b\bar{b}$ for the W'^{+} and the semileptonic decay of $t\bar{t}$, namely $\ell^{\pm}\not{E}_{T}jjb\bar{b}$, for the Z'. The missing energy $\not{E}_{T}$ is carried off by a neutrino in the top quark decay. The dominant backgrounds are also computed and assessments are presented for the W' and Z' discovery potential. After we impose kinematic cuts and reconstruct the final states, we conclude that a Z' resonance with mass 1 TeV could be seen above the SM $t\bar{t}$ background with a statistical significance more than 5 standard deviations (5σ) for 10 fb^{-1} integrated luminosity at 14 TeV, provided its coupling $g_{V} \equiv \sqrt{g_{L}^{2} + g_{R}^{2}}$ to the SM quarks is about 0.4, consistent with bounds from Tevatron searches in the dijet final state. The W' signal can be much larger than the SM background if a coupling strength 0.4 to the SM quarks is assumed. For purposes of comparison, the couplings of the SM W boson to SM quarks are $g_{L}^{Wu\bar{d}} = 0.461$ and those of the SM Z boson are $g_{L}^{Zu\bar{u}} = -0.257$, $g_{R}^{Zu\bar{u}} = 0.115$, $g_{L}^{Zd\bar{d}} = 0.314$ and $g_{R}^{Zd\bar{d}} = -0.057$.

Section IV is devoted to the measurement of the top quark polarization and the determination of the handedness of the new gauge bosons. We apply our approach to three benchmark models, the sequential SM-like W'/Z' model (SSM), the top-flavor model, and the left-right symmetric model (LRM). These models provide different predictions for the left-handed fraction of the coupling strengths of the new gauge bosons. We show that the coupling of a W' to tb can be determined precisely, whereas the uncertainty is relatively large for a Z' to $t\bar{t}$, owing mainly to better statistics and smaller SM backgrounds in the W' case. For $m_{W'}$ $(\simeq m_{Z'}) \sim 1$ TeV, our determinations of the handedness of the W' and Z' couplings allow the three benchmark models be separated to varying degrees with 100 fb^{-1} of accumulated data. With this large data sample, one can distinguish the Z' models if the central values of their top quark polarizations differ by $\sim 20\%$. For a leptophobic Z', one can differentiate among different models if the difference of the handedness of the coupling
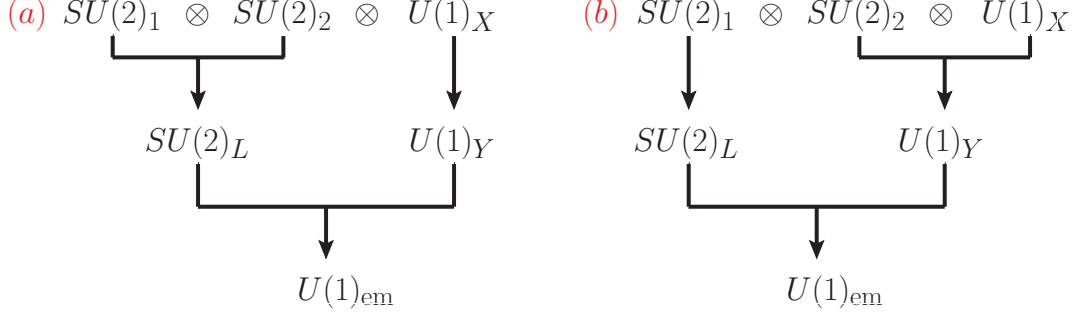
FIG. 1: Pictorial illustration of symmetry breaking patterns of $G(221)$ model.

to SM quarks is $\gtrsim 10\%$ (for coupling strength ~ 0.4)). Our overall summary is found in Sec. V.

II. MODELS WITH EXTRA GAUGE BOSONS

Extra gauge bosons may be classified according to their electromagnetic charges: W' (charged bosons) and Z' (neutral bosons). While a Z' can originate from an additional abelian $U(1)$ group, a W' arises often in models with an extra non-abelian group. In this section we consider the so-called $G(221)$ model [22] which carries the simplest non-abelian extension to the SM

$$G(221) = SU(2)_1 \otimes SU(2)_2 \otimes U(1)_X. \tag{1}$$

The model represents a typical gauge structure of many interesting NP models such as the non-universal model (NU) [23–25], the ununified (UU) model [26, 27], the fermiophobic (FP) model [28], left-right (LR) models [29], and so forth. Both W' and Z' bosons appear after the $G(221)$ symmetry is broken to the SM symmetry $G_{SM} = SU(2)_L \otimes U(1)_Y$. As depicted in Fig. 1, these models can be categorized by two symmetry breaking patterns,

(a) In the UU and NU models:

$U(1)_X$ is identified as the $U(1)_Y$ of the SM. The first stage of symmetry breaking $SU(2)_1 \times SU(2)_2 \to SU(2)_L$ occurs at the TeV scale, while the second stage of symmetry breaking $SU(2)_L \times U(1)_Y \to U(1)_{em}$ occurs at the electroweak scale;

(b) In the FP and LR models:

$SU(1)_1$ is identified as the $SU(2)_L$ of the SM. The first stage of symmetry breaking

$SU(2)_2 \times U(1)_X \to U(1)_Y$ occurs at the TeV scale, while the second stage of symmetry breaking $SU(2)_L \times U(1)_Y \to U(1)_{em}$ occurs at the electroweak scale.

In the first pattern the couplings of new gauge bosons to the SM fermions are predominately left-handed while in the second pattern the couplings are right-handed. A measurement of the polarization of the fermions from the new gauge bosons would decipher the handedness of the couplings.

Rather than focusing on a specific model, we explore the discovery potential of W' and Z' bosons in a model independent method, and we comment on a few new physics models later. The most general interaction of the Z' and W' to the SM quarks is

$$
\begin{aligned}
\mathcal{L} &= \bar{q}\gamma^{\mu}(g_L^{Z'} P_L + g_R^{Z'} P_R)q \ Z'_{\mu} \\
&+ \bar{q}\gamma^{\mu}(g_L^{W'} P_L + g_R^{W'} P_R)q' \ W'^{+}_{\mu} + h.c.
\end{aligned}
\tag{2}
$$

where $P_{L/R}$ is the usual left- and right-handed projector and q denotes the SM quarks. The Z' and W' are understood here to be color singlet states, but one can easily obtain the interaction of color octet bosons, such as a G', from insertion of the $SU(3)_C$ color matrices $\lambda_A/2$ in Eq. (2).

The masses of the W' and Z' are not necessarily equal. The mass difference between the W' and Z' can be generated either by symmetry breaking or through mixing with SM gauge bosons. The couplings $g_{L/R}^{Z'}$ and $g_{L/R}^{W'}$ usually are not independent when the W' and Z' originate from the same gauge group. For example, in the left-right model, the SM right-handed quark singlets form a doublet (u_R, d_R) which is gauged under the additional $SU(2)_R$ group. The W' and Z' transform as a $SU(2)_R$ triplet and their couplings to the SM quarks are correlated.

In this work we first treat $g_{L/R}^{W'}$ and $g_{L/R}^{Z'}$ as independent in our collider simulation to derive the experimental sensitivity on Z' and W' measurements. We then consider the correlation between the two couplings and masses in the context of some NP models. We use $g_{L/R}$ to denote the left-handed and right-handed couplings of the W' and Z' to the SM quarks. For simplicity we assume the couplings of Z' to up- and down-type quarks are the same.

For illustration we study three benchmark NP models in this work:

- sequential SM-like W'/Z' (SSM) model: the W' and Z' couplings to SM fermions are exactly the same as the SM W and Z boson, and $m_{W'} = m_{Z'}$. Although it is difficult

TABLE I: Couplings of a W' to tb and a Z' to $t\bar{t}$ for the sequential SM-like W'/Z' (SSM) model, the left-right symmetric model (LRM), and the top-flavor model, where s_w (c_w, t_w) = $\sin\theta_w$ ($\cos\theta_w$, $\tan\theta_w$), θ_w is the weak mixing angle, $g_2 = e/s_w$ is the weak coupling, $\alpha_{LR} \simeq 1.6$, and $\sin\tilde{\phi}$ is taken to be $1/\sqrt{2}$.

	$W'tb$	$Z't\bar{t}$
SSM	$\frac{g_2}{\sqrt{2}}\bar{b}\gamma_\mu P_L t W'^\mu$	$\frac{g_2}{6c_w}\bar{t}\gamma_\mu((-3+4s_w^2)P_L + 4s_w^2 P_R)t Z'^\mu$
LRM	$\frac{g_2}{\sqrt{2}}\bar{b}\gamma_\mu P_R t W'^\mu$	$\frac{g_2 t_w}{6}\bar{t}\gamma_\mu(\frac{1}{\alpha_{LR}}P_L + (\frac{1}{\alpha_{LR}} - 3\alpha_{LR})P_R)t Z'^\mu$
Top-Flavor	$\frac{g_2\sin\tilde{\phi}}{\sqrt{2}}\bar{b}\gamma_\mu P_L t W'^\mu$	$\frac{g_2\sin\tilde{\phi}}{\sqrt{2}}\bar{t}\gamma_\mu P_L t Z'^\mu$

in a realistic model to have couplings which are the same as in the SM, we show such a case for comparison.

- top-flavor model [24]: the W' and Z' couplings are purely left-handed, and $m_{W'} = m_{Z'}$.

- left-right symmetric model (LRM) [29]: Here, we consider a $SU(2)_L \times SU(2)_R \times U(1)_{B-L}$ model. The W' couplings to SM quarks are purely right-handed while the Z' couplings are dominantly right-handed. The difference of $m_{Z'}$ and $m_{W'}$ depends on the model parameter α_{LR}.

Table I is a summary of the couplings of a W' and a Z' to SM third generation quarks in these models. The couplings to the quarks of first two generations are the same, except that one should replace $\sin\tilde{\phi}$ by $\cos\tilde{\phi}$ in the top-flavor model.

A. Bounds on masses and couplings

The masses and couplings of Z' and W' bosons are bounded by various low energy measurements (mainly via the four-fermion operators induced by exchanges of new heavy gauge bosons) such as the precision measurements at the Z-pole at LEP-I [30], the W-boson mass [30], the forward-backward asymmetry in $b\bar{b}$ production at LEP-II [30], νe scattering [31], atomic parity violation [32–34], Moller scattering [35], and so forth. The bounds are severe when new gauge bosons couple to leptons directly, but they can be relaxed for a leptophobic model, as analyzed in Ref. [22].

Tevatron data place a lower bound about 1.1 TeV on the mass of a W' [36] and about 1.07 TeV for a Z' [37], based on the charged lepton plus missing energy ($\ell^{\pm} \not{E}_T$) and $\mu^+ \mu^-$ final states, respectively, with the assumption that the couplings between the W'/Z' and the SM fermions are the same as those in the SM. Searches for the W' and Z' at the Tevatron in dijet events yield lower bounds on $m_{W'}$ and $m_{Z'}$, assuming SM couplings, of 840 GeV and 740 GeV, respectively [38]. Recent CMS and ATLAS collaboration searches for a Z' from dilepton final states and a W' from lepton plus missing energy events place lower bounds $m_{Z'} > 1.14$ TeV (CMS) [39], along with $m_{W'} > 1.58$ TeV (CMS) [40] and $m_{W'} > 1.49$ TeV (ATLAS) [41]. The analyses assume the Z' and W' have sequential standard model couplings. CMS and ATLAS also present searches for a resonance in dijet events which also constrain the masses of a W' and a Z', but the lower bounds are looser than the Tevatron results [42, 43]. If the couplings between the W'/Z' and the SM particles are not small, one can expect the discovery of the these heavy resonances sooner or later at the LHC. Negative searches for a W'/Z' through the $t\bar{b}$ and $t\bar{t}$ final states at the Tevatron impose upper bounds on the production cross section times decay branching ratio ($\sigma_{W'} Br(W' \to t\bar{b})$, $\sigma_{Z'} Br(Z' \to t\bar{t})$) for masses up to 950 GeV and 900 GeV for W' and Z', respectively [44, 45].

III. LHC PHENOMENOLOGY

We divide our discussion of $W'^{\pm}$ and Z' phenomenology into two parts. In this section, we present our evaluation of the production cross sections and discuss the pertinent backgrounds with a view toward understanding the discovery potential of the two states. Section IV is then devoted to an examination of top quark polarization measurements as a means to learn more about the models that produce W' and Z' bosons.

We explore the W' in the $t\bar{b}/\bar{t}b$ decay mode, and the Z' in the $t\bar{t}$ mode. The production cross section of $q\bar{q} \to Z' \to t\bar{t}$ is

$$\sigma_{Z'}(\hat{s}) = \frac{\beta}{192\pi} \frac{\hat{s}}{(\hat{s} - m_{Z'}^2)^2 + m_{Z'}^2 \Gamma_{Z'}^2} \left[(g_L^2 + g_R^2)^2 (3 + \beta^2) + 6 g_L g_R (g_L^2 + g_R^2)(1 - \beta^2) \right], \quad (3)$$

where $\beta = \sqrt{1 - 4m_t^2/\hat{s}}$. The cross section of $q\bar{q}' \to W' \to t\bar{b}/\bar{t}b$ is

$$\sigma_{W'}(\hat{s}) = \frac{(1 - x_t^2)^2}{96\pi} \frac{\hat{s}}{(\hat{s} - m_{W'}^2)^2 + m_{W'}^2 \Gamma_{W'}^2} (g_L^2 + g_R^2)^2 \left(2 + x_t^2 \right), \quad (4)$$
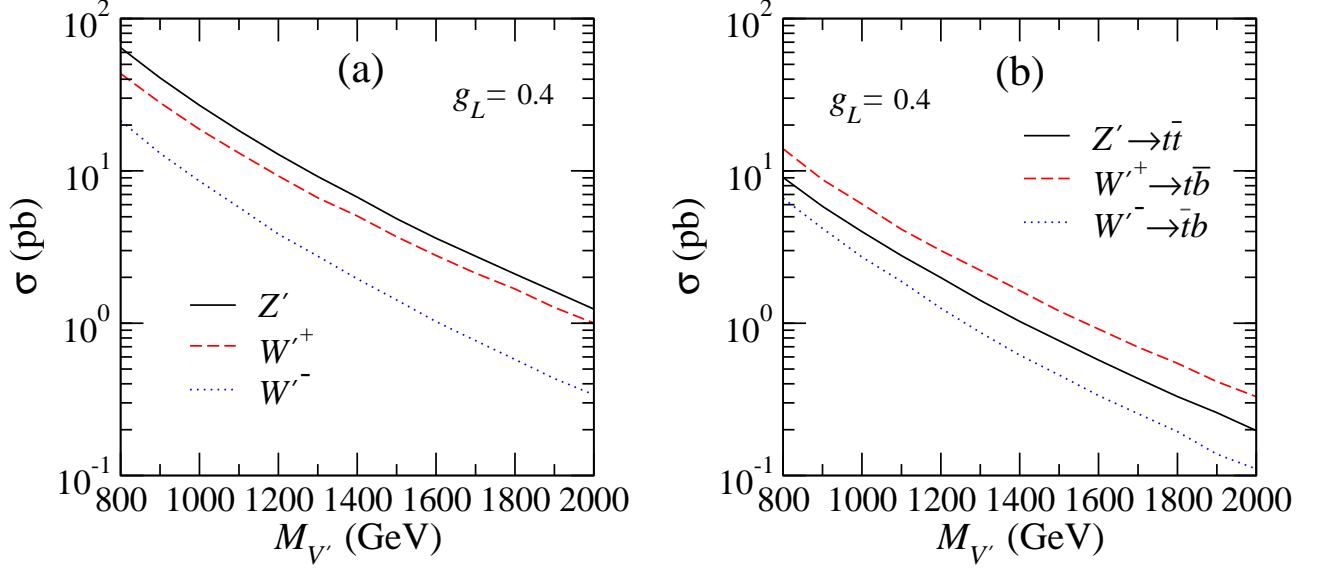
FIG. 2: Production cross sections of the W' and Z' at 14 TeV for the choice $g_L = 0.4$ and $g_R = 0$. The solid curves provide results before decay branching fractions are included, whereas the dashed curves include branching fractions.

where $x_t = m_t/\sqrt{\hat{s}}$. The partial decay width of $V' \to q\bar{q}'$ ($V' = W'$, Z') is

$$\Gamma(V' \to q\bar{q}') = \frac{m_{V'}}{8\pi}\beta_0 \left[(g_L^2 + g_R^2)\beta_1 + 6g_L g_R \frac{m_q m_{q'}}{m_{V'}^2}\right], \qquad (5)$$

where

$$\beta_0 = \sqrt{1 - 2\frac{m_q^2 + m_{q'}^2}{m_{V'}^2} + \frac{(m_q^2 - m_{q'}^2)^2}{m_{V'}^4}}, \qquad \beta_1 = 1 - \frac{m_q^2 + m_{q'}^2}{2m_{V'}^2} - \frac{(m_q^2 - m_{q'}^2)^2}{2m_{V'}^4}. \qquad (6)$$

Evaluations of the cross sections are presented in Fig. 2 at the LHC with center of mass energy 14 TeV. In the mass range of interest to us the W' and Z' bosons are much heavier than the top quark, and m_t can be ignored. Since the Z' and W' can decay into three generations of SM quarks, the decay branching ratio of $Z' \to t\bar{t}$ is about 1/6 while the ratio of $W' \to t\bar{b}$ is 1/3. The cross sections for other values of g_L and g_R can be obtained from the curves in Fig. 2 by a simple scaling, $\sigma_{V'} \propto (g_L^2 + g_R^2)$.

We use MadGraph/MadEvent [46] to obtain the signal and background distributions. These results are computed at leading order with the renormalization scale (μ_R) and factorization scale (μ_F) chosen as

$$\mu_R = \mu_F = \sqrt{m_t^2 + 2p_T^2(t)}. \qquad (7)$$

8

The CTEQ6.1L parton distribution functions (PDFs) [47] are used. The widths of W' and Z' for different g_L and g_R couplings are calculated in BRIDGE [48].

The coupling strength is set at $g_V \equiv \sqrt{g_L^2 + g_R^2} = 0.4$, which respects the dijet constraints at the Tevatron [38] in the leptophobic W'/Z' models with a universal coupling. We plot the production cross sections with the choice of $g_L = 0.4$, $g_R = 0$ in the figure. The curves shown in Fig. 2 also represent the cross sections for $g_R = 0.4$, $g_L = 0$. Our study can be extended easily to the case of other small couplings. The top quark polarization is sensitive only to the ratio of g_L and g_R, but statistical precision on the measurement of the top quark polarization requires a large enough coupling.

After including branching fractions, we also plot the cross sections for $pp \to Z'X \to t\bar{t}X$, $pp \to W'^+X \to t\bar{b}X$, and $pp \to W'^-X \to \bar{t}bX$. Universal couplings of the W'/Z' bosons to three generation of quarks are understood. Because the u-quark parton density in the proton is large, it is easy to understand that the Z' has the largest production cross section while the W'^- has the smallest one.

To be able to measure the top quark polarization, we focus on final states in which the top quark decays leptonically. Therefore, the W' search is via the channel $pp \to W'X \to tbX \to \ell^\pm \nu b\bar{b}X$. The Z' search is done in the channel $pp \to Z'X \to t\bar{t}X \to \ell^\pm \nu jjb\bar{b}X$. We consider semileptonic decay of only one of the top quarks in the $t\bar{t}$ mode of Z' decay because of its large branching ratio. One can also use the dilepton channel to search for a Z' using the MT2-assisted method discussed in Ref. [18, 19] to fully reconstruct the Z'.

A. Z' discovery potential

The collider signature of interest to us for the Z' boson is $\ell^\pm \nu jjb\bar{b}$, where one top quark decays semileptonically and the other decays hadronically. We consider in this subsection only μ^+ final states, $t \to b\mu^+\nu_\mu$, but the statistics will increase when the different flavors and charges of the leptons are combined. The major SM background is $t\bar{t}$ production via the QCD interaction. The sum of other backgrounds, such as $W/Z(\to \ell\ell)$+jets, single top, $W + b\bar{b}$, etc., is a factor of $\gtrsim 20$ smaller after the usual semileptonic $t\bar{t}$ selection cuts [49].

At the analysis level, all signal and background events are required to pass the acceptance cuts listed here:

$$p_T(\ell, j) > 20 \text{ GeV}, \qquad |\eta(\ell, j)| < 2.5, \qquad \Delta R_{jj,j\ell} > 0.4,$$

TABLE II: Cross sections (in fb) for the signal process $pp \to Z' \to t\bar{t} \to \mu^+ \not{E}_T jjb\bar{b}$ and the SM backgrounds at 14 TeV. Two b-jets are tagged. "With cuts" means the cross sections after all of the kinematic cuts, b-tagging and reconstruction. The universal coupling of the Z' to the SM quarks is set to be 0.4. The mass window cuts are $\Delta M = 150$ (200) GeV for a 1 (1.5) TeV Z' resonance, respectively.

	Z'_R			Z'_L			Background		
$M_{Z'}$	No cut	With cuts	ΔM	No cut	With cuts	ΔM	No cut	With cuts	ΔM
1 TeV	275.6	29.5	28.3	275.6	27.2	26.2	3.75×10^4	133.1	87.0
1.5 TeV	51.4	3.0	2.6	52.5	3.9	3.5	3.75×10^4	133.1	11.3

$$\not{E}_T > 30 \text{ GeV}, \quad H_T > 500 \text{ GeV}, \quad M_T > 800 \text{ GeV}, \tag{8}$$

where $p_T(\eta, \not{E}_T)$ denotes the transverse momentum (rapidity, missing transverse momentum), $\Delta R_{kl} \equiv \sqrt{(\eta_k - \eta_l)^2 + (\phi_k - \phi_l)^2}$ is the separation in the azimuthal angle (ϕ)-pseudorapidity (η) plane between the objects k and l, H_T is the scalar sum of the transverse momenta of the final state visible particles plus $\not{E}_T$, and M_T is the cluster transverse mass defined as $M_T \equiv \sqrt{\sum_{i=j,\ell} p_i^2 + \not{E}_T^2} + \not{E}_T$. We model detector resolution effects by smearing the final state energy according to $\delta E/E = \mathcal{A}/\sqrt{E/\text{GeV}} \oplus \mathcal{B}$, where we take $\mathcal{A} = 10(50)\%$ and $\mathcal{B} = 0.7(3)\%$ for leptons (jets). To account for b-jet tagging efficiencies, we demand two b-tagged jets, each with a tagging efficiency of 60%.

We consider two masses $m_{Z'} = 1$ TeV and 1.5 TeV and the coupling strength $g_{Z'} = 0.4$ to satisfy the bounds on heavy resonance searches in the dijet channel at the Tevatron. The cross sections for $t\bar{t}$ before and after the cuts are shown in Table II.

Since there is only one neutrino in the final state, the undetected z component of the neutrino momentum can be reconstructed from the on-shell condition of the W-boson. This procedure leads to a two-fold solution, but the ambiguity can be removed by the top quark on-shell condition $m_{b\ell\nu}^2 = m_t^2$, where $m_t = 173.3$ GeV [50] is used. If no real solution is obtained, we use the top quark on-shell condition first, and then the W-boson on-shell condition to choose the better solution. Since the b and $\bar{b}$ are indistinguishable, one must pick which b-jet should be combined with the charged lepton. We use the on-shell condition of the top quark in the hadronic decay to select one of the b-jets to pair with the two jets that are the decay products of W-boson. The efficiency for choosing the correct b-jets to
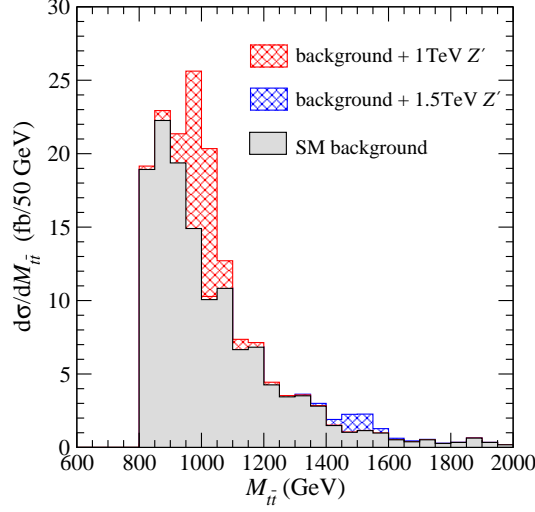
FIG. 3: Distribution in $m_{t\bar{t}}$ for a Z' and the SM $t\bar{t}$ background at the LHC. The coupling strength $g_{Z'}$ is set to be 0.4.
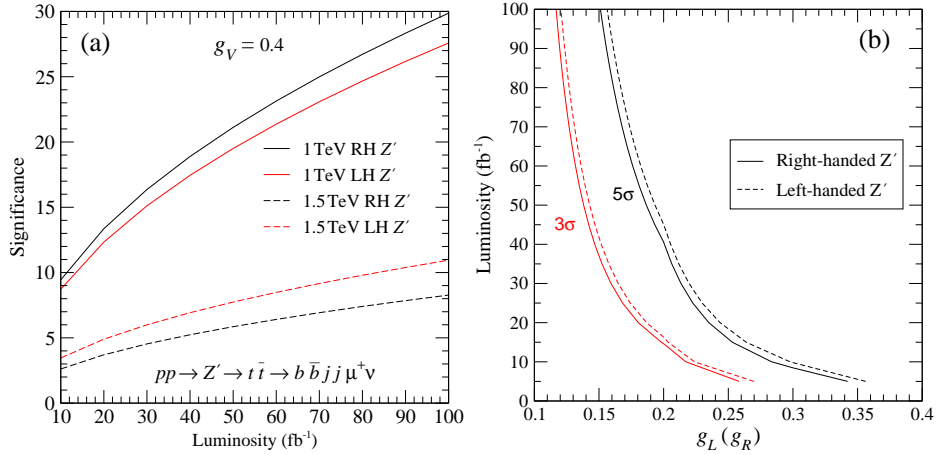

FIG. 4: (a) Discovery potential for a Z' boson at 14 TeV as a function of the integrated luminosity for a left-handed Z'-t-$\bar{t}$ coupling ($g_L = 0.4$, $g_R = 0$) or a right-handed coupling ($g_L = 0$, $g_R = 0.4$). (b) Luminosities required for 5 standard deviation (5σ) and 3 standard deviation (3σ) discovery if the Z' mass is 1 TeV, as a function of the coupling strength $g_L(g_R)$.

reconstruct the semileptonic and hadronic decays of the top quarks can reach $\gtrsim 99.7\%$.

In our simulations, after kinematic cuts and event reconstruction, the Z' resonance peak can be seen above the SM continuum in the $t\bar{t}$ invariant mass distribution, $m_{t\bar{t}}$, especially for a 1 TeV Z' . The results are shown in Fig. 3. To enhance the discovery significance we
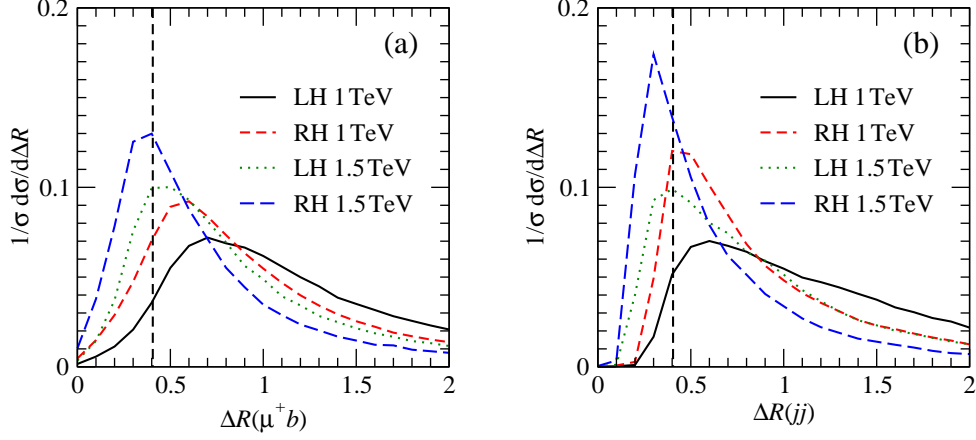
FIG. 5: (a) ΔR distributions for the μ^+ and b from t semileptonic decay. (b) ΔR distributions for two light jets from $\bar{t}$ hadronic decay. The vertical dashed line indicates the ΔR cut applied in our event selection.

further focus on the events within a mass window around the resonance:

$$|m_{t\bar{t}} - m_{Z'}| \leq 150 \ (200) \ \text{GeV, for 1 (1.5) TeV Z}' \tag{9}$$

Figure 4 shows the statistical significance $(S/\sqrt{B})$ for discovery as a function of accumulated luminosity for $m_{Z'} = 1$ TeV and $m_{Z'} = 1.5$ TeV, where S denotes the number of signal events while B number of background events. Since the charged lepton from a right-handed top quark decay is boosted to a harder p_T, more signal events survive after cuts in a right-handed Z' model (black-solid curve) than in a left-handed Z' model (red-solid curve). Therefore, the statistical significance for a right-handed Z' is better when $m_{Z'} = 1$ TeV. However, the situation reverses when the Z' becomes heavier because the selection cuts play a role. For a heavy enough Z', the top quark is highly boosted. The leptons and jets from its decay are collimated and fail the ΔR separation cuts, as can be seen in Fig. 5. The peak position in the ΔR distribution for two light jets shifts down below 0.4 when the mass of a right-handed Z' increases from 1 TeV to 1.5 TeV. As a result, the discovery potential for a very heavy, right-handed Z' is worse than for a left-handed Z', as illustrated in the black-dashed and red-dashed curves in Fig. 4 for a 1.5 TeV Z'.

12

TABLE III: Cross sections (in fb) for the signal process $pp \to W' \to t\bar{b} \to \mu^+ \not{E}_T b\bar{b}$ and the SM backgrounds at 14 TeV. Two b-jets are tagged. "With cuts" refers to cross sections after all of the kinematic cuts, b-tagging, and reconstruction. The value 0.4 is used for the universal coupling of the W' to the SM quarks. The mass window cuts are $\Delta M = 150$ (200) GeV for a 1 (1.5) TeV W', respectively.

	W'_R			W'_L			Background		
$M_{W'}$	No cut	With cuts	ΔM	No cut	With cuts	ΔM	No cut	With cuts	ΔM
1 TeV	652.1	109.4	105.2	650.3	112.9	108.5	3.04×10^4	412.1	8.4
1.5 TeV	131.7	23.9	22.7	129.2	26.1	24.8	3.04×10^4	412.1	2.0

B. W' discovery potential

The search for a W' in the tb mode involves the study of the $\ell^\pm b\bar{b}$ plus missing energy final state, where the missing energy originates from the neutrino in top quark decay. We examine only the W'^+ case since its production cross section is about a factor of two larger than W'^-. We demand that two jets are b-tagged. The SM background processes include production of single top quarks, $Wb\bar{b}$, Wjj, and $t\bar{t}$. Only the single-top background is considered in our study because it is about a factor of 10 larger than the others [51]. There are three single-t backgrounds: $q\bar{q}' \to t\bar{b}$ (named $t\bar{b}$), $qb \to q't$ (named bq) and $qg \to q't\bar{b}$ (called Wg-fusion). The bq channel has only one b-jet in the final state, but it is possible that the other light-favor jet is misidentified as a b-jet as well. The channel has a large cross section (~ 150 pb [52]). We also apply a mistagging rate for charm-quarks $\epsilon_{c\to b} = 10\%$ for $p_T(c) > 50\,\text{GeV}$. The mistag rate for a light jet is $\epsilon_{u,d,s,g\to b} = 0.67\%$ for $p_T(j) < 100\,\text{GeV}$ and 2% for $p_T(j) > 250\,\text{GeV}$. For $100\,\text{GeV} < p_T(j) < 250\,\text{GeV}$, we linearly interpolate the fake rates given above.

All signal and background events are required to pass the acceptance cuts:

$$p_T(\ell) > 20 \text{ GeV}, \quad |\eta(\ell)| < 2.5, \quad \not{E}_T > 25 \text{ GeV},$$
$$p_T(j) > 50 \text{ GeV}, \quad |\eta(j)| < 3.0, \quad \Delta R(jj) > 0.4, \quad \Delta R(j\ell) > 0.3 . \tag{10}$$

The notation is the same as in the Z' search. The event reconstruction is done in a manner similar to Ref. [51].

A two-fold solution may be obtained for the undetected z component of the momentum

of the missing neutrino if the W-boson on-shell condition is used. However, unlike $Z' \to t\bar{t}$, there is not a second top quark in the final state to help in selecting the correct b-jet to pair with the charged lepton. Instead, we use the top quark on-shell condition, $m_{b\ell\nu}^2 = m_t^2$ and loop over the two b-jets to find the better paring of the b-jet and charged lepton, and the better solution for the neutrino momentum. If no real solution is obtained, we discard the event. After the neutrino momentum is obtained, we can reconstruct the momenta of the top quark and the W'. To further suppress the SM backgrounds, we limit the event set to a mass window around the W' peak position. For a 1 TeV (1.5 TeV) resonance, we adopt

$$|m_{t\bar{b}} - m_{W'}| \leq 150 \ (200) \text{ GeV}. \tag{11}$$

After the cuts are imposed and the two b-jets are tagged, the SM backgrounds are at the fb level while the signal rates are about 100 (20) fb for W' masses of 1 (1.5) TeV. The signal and background cross sections are shown in Table III. After imposing the mass window cut and demanding two b-tagged jets, we find that the Wg-fusion channel yields the largest background. For a 1 TeV W', the single-t processes give these background rates: Wg-fusion, 6.3 fb; bq, 1.3 fb; $t\bar{b}$, 0.8 fb. For a 1.5 TeV W', the Wg-fusion rate is 1.4 pb, bq is 0.4 fb, and $t\bar{b}$ is 0.16 pb. The acceptance for a left-handed W' is slightly better than for a right-handed one. Because the top quark is boosted from W' decay, ΔR between the charged lepton and the b quark from the decay of a right-handed top quark is smaller than that from a left-handed top quark, similar to the situation described above for a 1.5 TeV Z'.

The coupling strength $g_L^{W'} = 0.4$ or $g_R^{W'} = 0.4$ is used in our analysis to satisfy constraints from the Tevatron dijet search. Since the background is much smaller than the signal rate, $S/B \simeq \mathcal{O}(10)$, a W'^+ should be easy to discover. Moreover, good accuracy can be obtained for the top quark polarization measurement, as discussed in the next section.

IV. TOP QUARK POLARIZATION

The symmetry breaking patterns mentioned in Sec. II prefer either a purely left-handed top quark $(SU(2)_1 \times SU(2)_2 \to SU(2)_L)$ or a purely right-handed top quark $(SU(2)_R \times U'_Y \to U(1)_Y)$. We can measure the top quark polarization from the $\cos\theta$ distribution of the charged lepton in top quark decay after the top quark kinematics are reconstructed in the W'^+ and Z' final states, as described in Sec. III.
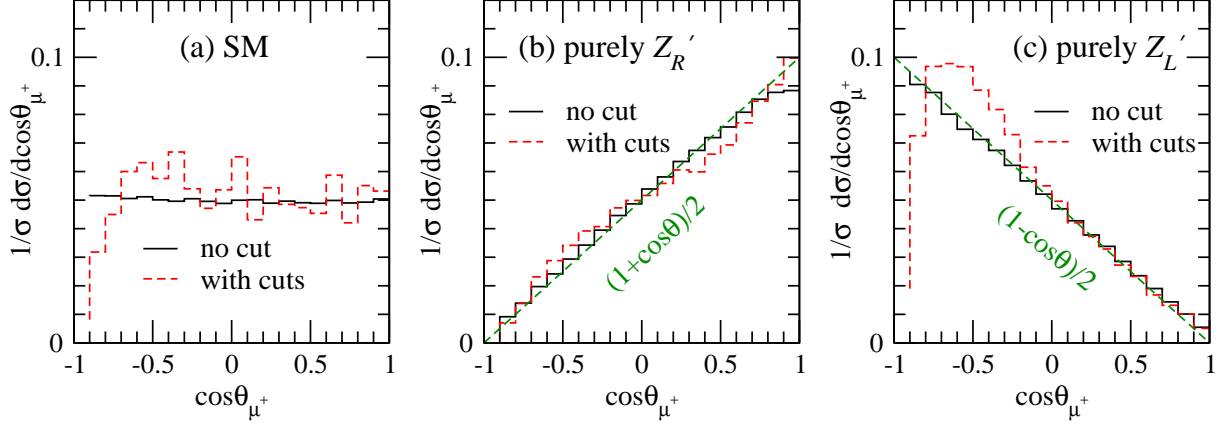
FIG. 6: Distributions in $\cos\theta_\ell$ of the lepton from the decay of top quarks produced in $t\bar{t}$ events before and after cuts: (a) SM, (b) right-handed polarized top quarks in Z' decay; (c) left-handed polarized top quarks in Z' decay. The distributions for W' decay are similar to those for Z' decay.

Figure 6 displays the $\cos\theta_\ell$ distributions of the μ^+ in the rest frame of the top quark in $t\bar{t}$ events for the SM background and for a 1 TeV Z' boson before and after cuts. A top quark produced at the LHC via QCD interactions is unpolarized, as shown by the flat black curve in Fig. 6 (a). We see the $1 \pm \cos\theta_\ell$ behaviors in Fig. 6(b) and (c) for purely right- and left-handed polarized top quarks from Z' decay. After kinematic cuts are imposed, the distributions are distorted and drop significantly in the region $\cos\theta_\ell \sim -1$, affected mainly by the p_T and ΔR cuts. However, the main characteristic features remain, i.e. flatness and $1 \pm \cos\theta_\ell$. While not shown here, the $\cos\theta_\ell$ distributions in right- and left-handed W' decay are similar to the Z' case.

We denote the distributions from purely left-handed (right-handed) top quarks $F_L(y)$ $(F_R(y))$ where $y = \cos\theta_\ell$. These are the distributions in Fig. 6 (b) and (c) before and after cuts. We use these as the basis functions to fit the event distributions from our simulations of various models. We adopt a general linear least-squares fit in this study to estimate how well the degree of top quark polarization can be determined.

An observed angular distribution $O(y)$ after the SM background is subtracted can be expressed as

$$O(y) = \epsilon_L \, F_L(y) + \epsilon_R \, F_R(y), \tag{12}$$

where ϵ_L (ϵ_R) is the fraction of left-handed (right-handed) top quarks. The values of ϵ_L and

ϵ_R are chosen as the best parameters that minimize χ^2, defined as

$$\chi^2 = \sum_{i=1}^{N} \left[\frac{O(y_i) - \epsilon_L F_L(y_i) - \epsilon_R F_R(y_i)}{\sigma_i} \right]^2, \tag{13}$$

where N is the number of bins, and $\sigma_i = \sqrt{O(y_i)}$ is the statistical error (standard deviation) of the ith data point. The minimum of Eq. 13 occurs where the derivative of χ^2 with respect to both ϵ_L and ϵ_R vanishes, yielding the normal equations of a least-squares problem:

$$0 = \sum_{i=1}^{N} \frac{1}{\sigma_i^2} \left[O(y_i) - \epsilon_L F_L(y_i) - \epsilon_R F_R(y_i) \right] F_l(y_i), \quad \text{where} \ \ l = L(R). \tag{14}$$

Interchanging the order of summations, one can write the above equations as matrix equations,

$$\alpha_{LL}\epsilon_L + \alpha_{LR}\epsilon_R = \beta_L, \qquad \alpha_{RL}\epsilon_L + \alpha_{RR}\epsilon_R = \beta_R, \tag{15}$$

where

$$\alpha_{lm} = \sum_{i=1}^{N} \frac{F_l(y_i)F_m(y_i)}{\sigma_i^2}, \qquad \beta_l = \sum_{i=1}^{N} \frac{O(y_i)F_l(y_i)}{\sigma_i^2}. \tag{16}$$

The coefficients ϵ_L and ϵ_R can be obtained from Eq. 15 as

$$\epsilon_l = \sum_{m=L}^{R} [\alpha_{lm}]^{-1}\beta_m = \sum_{m=L}^{R} C_{lm} \left[\sum_{i=1}^{N} \frac{O(y_i)F_m(y_i)}{\sigma_i^2} \right], \quad l = L, R . \tag{17}$$

The inverse matrix $C_{lm} \equiv [\alpha_{lm}]^{-1}$ is closely related to the standard uncertainties of the estimated coefficients ϵ_L and ϵ_R. Assuming the data points are independent, consideration of propagation of errors shows that the variance σ_f^2 in the value of ϵ_l is

$$\sigma^2(\epsilon_l) = \sum_{i=1}^{N} \sigma_i^2 \left(\frac{\partial \epsilon_l}{\partial O(y_i)} \right)^2 = C_{ll}, \tag{18}$$

i.e. the diagonal elements of $[C]$ are the variances (squared uncertainties) of the fitted coefficients.

We illustrate this method with two toy models in which the $W'tb$ couplings are $\epsilon_L = 30\%$ and $\epsilon_L = 70\%$, where the fraction of left-handed top quarks is closely related to the W'-t-$\bar{b}$ coupling as

$$\epsilon_L \equiv \frac{\sigma(t_L)}{\sigma(t_L) + \sigma(t_R)} \approx \frac{g_L^2}{g_L^2 + g_R^2}. \tag{19}$$

For simplicity, we choose the same ϵ_L for the $Z'tt$ coupling as for $W'tb$. (Note that $\epsilon_L \approx 1 - \epsilon_R$.) The coupling strength to the top quark ($g_V = \sqrt{g_L^2 + g_R^2}$) and the masses of the Z'

and W' are taken to be the same: $g_V^{Z'} = g_V^{W'} = 0.4$; $m_{Z'} = m_{W'} = 1$ TeV. We also adopt 5% uncertainties in each bin to take into account the imperfect predictions of the template distributions $F_L(y)$ and $F_R(y)$. [2] We generate ten bins of data in the $\cos\theta_\ell$ distribution. The first bin, $\cos\theta_\ell \sim -1$, is not used in the fits because of the significant drop-off associated with cuts.

Our results for ϵ_L in our toy models are shown in Fig. 7 with the legends "True (30,30)" and "True (70,70)". For an assumed $\epsilon_L = 30\%$ (70%) used in the event generation, the measured polarization (ϵ_L^{mea}) is found to be $\epsilon_L^{mea} = 31.4\% \pm 15\%$ ($68.5\% \pm 15\%$) for a Z', and $\epsilon_L^{mea} = 30.2\% \pm 3.4\%$ ($70.2\% \pm 3.4\%$) for a W' for an integrated luminosity of 10 fb^{-1}. The uncertainties are reduced to 10.5% and 2.1% for a Z' and a W', respectively, if the integrated luminosity is raised to 100 fb^{-1}, while the central values remain the same. As shown in the figure, ϵ_L can be measured precisely in the $W' \to t\bar{b}$ mode, owing to the small SM backgrounds, while the measurement in the $Z' \to t\bar{t}$ channel is less accurate because of the large $t\bar{t}$ background.

The statistical uncertainty of each bin in the $\cos\theta_\ell$ distribution scales as $\sqrt{N_i} = \sqrt{\sigma_i \mathcal{L}}$ where σ_i is the differential cross section of the i-th bin. An increase of the luminosity by a factor of k reduces the uncertainties by a factor of $\sqrt{k}$.

Discovery of the Z' and W' bosons might not occur together owing to different collider signatures and SM backgrounds. For example, it is easier in general to observe the W' boson at the LHC as it exhibits simpler collider signatures and smaller SM backgrounds than the Z'. We use our simulated events to determine how well ϵ_L could be measured for the W' and for the Z'. For the three benchmark NP models described in Sec. II, we obtain the results shown in Table IV. All the fitted central values are close to the true values in each model. We emphasize that the values of ϵ_L are determined independently for the W' and the Z'.

The polarization of the top quark in W' decay can be measured precisely. The uncertainty is $\lesssim 5\%$ in $\epsilon_L^{W'}$ for 10 fb^{-1} of integrated luminosity. It decreases to $\lesssim 3\%$ for 100 fb^{-1} of integrated luminosity. The polarization is measured less accurately in the $t\bar{t}$ channel, however, because the SM $t\bar{t}$ background is large. For a Z' in the SSM and top-flavor models, the uncertainties are about 30% and 24% with 10 fb^{-1} of integrated luminosity, respectively.

---

[2] The 5% variation may be too optimistic, but the value to be adopted will not be obvious until a more precise next-to-leading order calculation is done.

TABLE IV: Fitted values of ϵ_L for W' and Z' boson production at the LHC (14 TeV) with integrated luminosities of $10\,\mathrm{fb}^{-1}$ and $100\,\mathrm{fb}^{-1}$. We fix $m_{W'} = 1\,\mathrm{TeV}$ for all three models and vary $m_{Z'}$ correspondingly: $m_{W'} = m_{Z'}$ for the SSM and Top-Flavor models while $m_{Z'} = 1.2$ TeV for the LRM model with $\alpha_{LR} = 1.6$.

Z'	Theory	Measured $\epsilon_L(\%)$	
	$\epsilon_L(\%)$	$10\,\mathrm{fb}^{-1}$	$100\,\mathrm{fb}^{-1}$
LRM	2.0	3.0 ± 70.9	3.0 ± 40.1
SSM	83.6	86.7 ± 30.1	86.7 ± 20.2
Top-Flavor	100.0	101.9 ± 23.8	101.9 ± 16.7
W'	Theory	Measured $\epsilon_L(\%)$	
	$\epsilon_L(\%)$	$10\,\mathrm{fb}^{-1}$	$100\,\mathrm{fb}^{-1}$
LRM	0.0	5.1 ± 3.7	5.1 ± 2.5
SSM	100.0	101.4 ± 4.1	101.4 ± 1.7
Top-Flavor	100.0	101.3 ± 4.5	101.3 ± 1.8

They are reduced to about 20% and 17% when the integrated luminosity is increased to $100\,\mathrm{fb}^{-1}$. For a Z' in the LRM, the uncertainty is large, $\sim 70\%$ for $10\,\mathrm{fb}^{-1}$ and $\sim 40\%$ for $100\,\mathrm{fb}^{-1}$ integrated luminosities. The larger uncertainties arise because Z' mass is heavier (1.2 TeV) and the coupling of the Z' to $t\bar{t}$ is smaller than in the SSM and top-flavor models, as noted in Table I. The statistics are too low to obtain a good fit.

The fitted uncertainties are generally larger for a left-handed Z'_L compared with a right-handed Z'_R if the the masses and couplings to the top quark are the same, because the charged lepton from the decay of a left-handed top quark is softer than from a right-handed top quark. Therefore, the statistics are usually greater for a Z'_R. However, the situation switches when the Z' is heavier, because the separation ΔR computed from the charged lepton and the b from top quark decay will more easily fail the kinematic cuts, as shown in Sec. III A.

It is of also of interest to consider the correlation between the W' and Z' bosons as it could be used to discriminate different NP models. Assuming both bosons are discovered at the LHC, we examine the correlation of the polarization of top quarks produced in W' and Z' boson decays in the three NP models. The results are shown in Fig. 7 for $m_{W'} = 1$ TeV. In

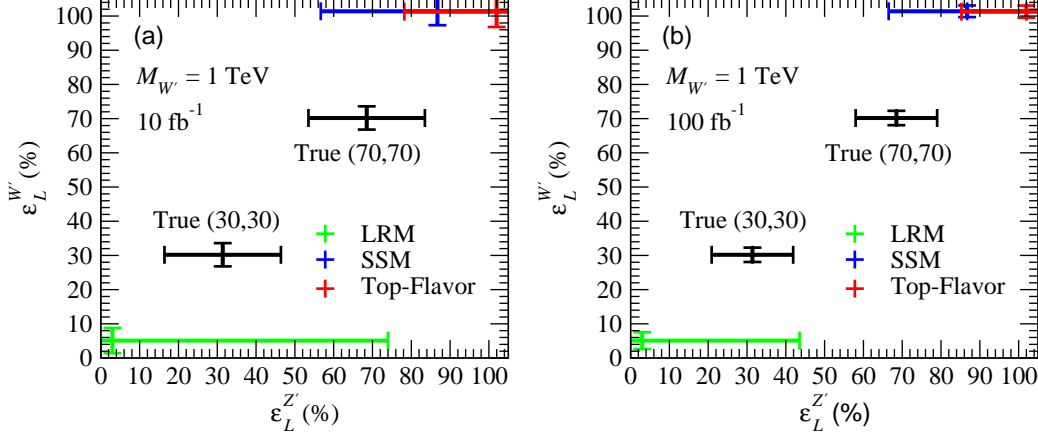FIG. 7: Top quark polarizations determined from χ^2 fits in $pp \to W'^+ \to t\bar{b}$ and $pp \to Z' \to t\bar{t}$ for two assumed t-polarizations $\epsilon_L = 0.3$, 0.7. The results for benchmark models, the left-right symmetric model (LRM), the sequential standard model (SSM where couplings are the same as the SM W and Z bosons), and the top-flavor model, are also shown. The uncertainties are the quadratic sum of the uncertainties from statistics and theory and are shown as black and red bands for integrated luminosities of 10 fb^{-1} and 100 fb^{-1}, respectively.

the SSM and top-flavor models $m_{Z'} = m_{W'}$, while in the LRM $m_{Z'} \simeq 1.2\, m_{W'}$ for $\alpha_{LR} = 1.6$.

V. DISCUSSION AND SUMMARY

Extra gauge bosons may be among the new states produced at the LHC. Depending on how the gauge group is broken in the BSM scenario and how the SM fermions are charged, the couplings of the heavy gauge bosons W' and Z' to the SM fermions could have the same or different handedness. While it may be more straightforward to discover the W'/Z' through their dijet or leptonic decays, we emphasize that decays into top quark final states allow us to study the nature of the coupling between the new gauge bosons and the SM quarks. These channels are also complementary to the dijet and leptonic channels, especially for leptophobic W'/Z' bosons.

We focus on final states in which the W'^+ boson decays into a top quark and a bottom quark and the Z' boson decays into a top-antitop quark pair. The collider signatures we examine are $\ell^+ \not{E}_T b\bar{b}$ for the W'^+ and the semileptonic channel $\ell^\pm \not{E}_T jjb\bar{b}$ for the Z'. The missing energy $\not{E}_T$ is carried off by a neutrino in the top quark decay. After an event simula-

19

tion of the signals and backgrounds, and imposing a set of kinematic cuts, we reconstruct the momentum of the missing neutrino using on-shell conditions for the W boson and the top quark. Adopting a coupling strength $g_V = \sqrt{g_L^2 + g_R^2} = 0.4$ (g_L and g_R are the left-handed and right-handed $Z't\bar{t}$ couplings) consistent with data from the Tevatron dijet search, we find that a 1 TeV Z' resonance could be seen above the SM $t\bar{t}$ background at 14 TeV with a statistical significance of more than 5σ for 10 fb^{-1} of integrated luminosity. The W' signal can be much larger than the SM background if the coupling strength of the W' to the SM quarks is not too small (~ 0.4).

Even in the presence of SM backgrounds and despite distortions associated with cuts, we show that the left-right handedness of the top quark can be measured from the angular distribution in $\cos\theta_\ell$ of the charged lepton in the top quark rest frame. This observable is most interesting because it reflects the coupling structure of the W'/Z' to the top quark. When performing χ^2 fits to our simulated $\cos\theta_\ell$ distributions, we allow 5% fluctuations in each bin of $\cos\theta_\ell$. In the W' case, the SM backgrounds are small and our fits result in uncertainties of $\lesssim 5\%$ for the fraction of left-handed coupling for 10 fb^{-1} of accumulated luminosity. The Z' situation is less good because the statistics are smaller and the SM backgrounds are larger. The uncertainty for the Z' decreases from $\sim 15\%$ to $\sim 10\%$ when the integrated luminosity is increased from 10 fb^{-1} to 100 fb^{-1}.

We apply our approach to three benchmark models, the SSM, LRM, and top-flavor models. The central values from our fits are close to the true values in these models, with a deviation about $2\% \sim 5\%$, and they are insensitive to luminosity. The uncertainties, again, are small for W' and larger for Z', depending mainly on statistics. Owing to the larger uncertainty in the Z' case and the similarity in the handedness of couplings (true values $\epsilon_L \simeq 84\%$ for SSM and $\epsilon_L = 100\%$ for top-flavor model), the SSM and top-flavor models can be separated only marginally with 100 fb^{-1} of integrated luminosity when the Z' and W' results are combined, as shown in Fig. 7. However, the situation is better if the Z' is leptophobic and the coupling strength to SM quarks is as large as 0.4. This is the case we show first using toy models with the couplings $\epsilon_L = 30\%$ and 70% in Fig. 7. Since the uncertainty can be reduced to about 10%, one could distinguish models with handedness of couplings to SM quarks differing by about 10%.

We remark that the coupling strength of a W'/Z' to the top quark cannot be determined from our study since our signal cross sections also depend on the couplings of the W'/Z'

to light quarks. Finally, our approach relies on reliable calculations for the backgrounds as well as the signals, which are crucial for normalizations and the kinematic distributions. Next-to-leading order (NLO) QCD contributions enhance the cross section significantly [53], possibly improving our results. The higher order QCD contributions to the SM backgrounds are also not negligible. A study that consistently includes higher order contributions to both the backgrounds and the signals is needed, and we leave it for future work.

[1] R. W. Robinett and J. L. Rosner, Phys. Rev. **D25**, 3036 (1982).

[2] P. Langacker, R. W. Robinett, and J. L. Rosner, Phys. Rev. **D30**, 1470 (1984).

[3] V. D. Barger, N. G. Deshpande, J. L. Rosner, and K. Whisnant, Phys. Rev. **D35**, 2893 (1987).

[4] D. London and J. L. Rosner, Phys. Rev. **D34**, 1530 (1986).

[5] J. L. Rosner, Phys. Rev. **D35**, 2244 (1987).

[6] W. J. Marciano and J. L. Rosner, Phys. Rev. Lett. **65**, 2963 (1990).

[7] J. L. Rosner, Phys. Rev. **D54**, 1078 (1996).

[8] J. L. Rosner, Phys. Lett. **B387**, 113 (1996).

[9] M. S. Carena, A. Daleo, B. A. Dobrescu, and T. M. P. Tait, Phys. Rev. **D70**, 093009 (2004).

[10] T. G. Rizzo, JHEP **05**, 037 (2007).

[11] F. Petriello and S. Quackenbush, Phys. Rev. **D77**, 115004 (2008).

[12] P. Langacker, Rev. Mod. Phys. **81**, 1199 (2009), and the references therein.

[13] C.-W. Chiang, N. G. Deshpande, X.-G. He, and J. Jiang, Phys. Rev. **D81**, 015006 (2010).

[14] F. del Aguila *et al.*, Phys. Lett. **B685**, 302 (2010).

[15] R. Diener, S. Godfrey, and T. A. W. Martin, arXiv:1006.2845.

[16] M. Frank, A. Hayreter, and I. Turan, Phys. Rev. **D83**, 035001 (2011).

[17] C. Grojean, E. Salvioni, and R. Torre, arXiv:1103.2761.

[18] E. L. Berger, Q.-H. Cao, C.-R. Chen, G. Shaughnessy, and H. Zhang, Phys. Rev. Lett. **105**, 181802 (2010).

[19] H. Zhang, E. L. Berger, Q.-H. Cao, C.-R. Chen, and G. Shaughnessy, Phys. Lett. **B696**, 68 (2011).

[20] M. Jezabek and J. H. Kuhn, Phys. Lett. **B329**, 317 (1994).

[21] G. Mahlon and S. J. Parke, Phys. Rev. **D53**, 4886 (1996).

[22] K. Hsieh, K. Schmitz, J.-H. Yu, and C.-P. Yuan, Phys. Rev. **D82**, 035011 (2010).

[23] X. Li and E. Ma, Phys. Rev. Lett. **47**, 1788 (1981).

[24] E. Malkawi, T. M. P. Tait, and C. P. Yuan, Phys. Lett. **B385**, 304 (1996).

[25] X.-G. He and G. Valencia, Phys. Rev. **D66**, 013004 (2002).

[26] H. Georgi, E. E. Jenkins, and E. H. Simmons, Phys. Rev. Lett. **62**, 2789 (1989).

[27] H. Georgi, E. E. Jenkins, and E. H. Simmons, Nucl. Phys. **B331**, 541 (1990).

[28] V. D. Barger, W.-Y. Keung, and E. Ma, Phys. Rev. **D22**, 727 (1980).

[29] G. Senjanovic and R. N. Mohapatra, Phys. Rev. **D12**, 1502 (1975).

[30] Particle Data Group, K. Nakamura *et al.*, J. Phys. **G37**, 075021 (2010).

[31] CHARM-II Collaboration, P. Vilain *et al.*, Phys. Lett. **B364**, 121 (1995).

[32] P. Vetter, D. Meekhof, P. Majumder, S. Lamoreaux, and E. Fortson, Phys. Rev. Lett. **74**, 2658 (1995).

[33] C. Wood *et al.*, Science **275**, 1759 (1997).

[34] J. Guena, M. Lintz, and M. Bouchiat, physics/0412017.

[35] SLAC E158 Collaboration, P. Anthony *et al.*, Phys. Rev. Lett. **95**, 081601 (2005).

[36] CDF Collaboration, T. Aaltonen *et al.*, Phys. Rev. **D83**, 031102 (2011).

[37] CDF Collaboration, T. Aaltonen *et al.*, arXiv:1101.4578.

[38] CDF Collaboration, T. Aaltonen *et al.*, Phys. Rev. **D79**, 112002 (2009).

[39] CMS Collaboration, arXiv:1103.0981.

[40] CMS Collaboration, arXiv:1103.0030.

[41] ATLAS Collaboration, arXiv:1103.1391.

[42] ATLAS Collaboration, G. Aad *et al.*, Phys. Rev. Lett. **105**, 161801 (2010).

[43] CMS Collaboration, V. Khachatryan *et al.*, Phys. Rev. Lett. **105**, 211801 (2010).

[44] CDF Collaboration, T. Aaltonen *et al.*, Phys. Rev. Lett. **100**, 231801 (2008).

[45] CDF Collaboration, T. Aaltonen *et al.*, Phys. Rev. Lett. **103**, 041801 (2009).

[46] J. Alwall *et al.*, JHEP **09**, 028 (2007).

[47] J. Pumplin *et al.*, JHEP **07**, 012 (2002).

[48] P. Meade and M. Reece, hep-ph/0703031.

[49] ATLAS, G. Aad *et al.*, arXiv:0901.0512.

[50] CDF and D0 Electroweak working group, arXiv:1007.3178.

[51] S. Gopalakrishna, T. Han, I. Lewis, Z.-G. Si, and Y.-F. Zhou, Phys. Rev. **D82**, 115020 (2010).

[52] R. Schwienhorst, C.-P. Yuan, C. Mueller, and Q.-H. Cao, Phys. Rev. **D83**, 034019 (2011).

[53] Z. Sullivan, Phys. Rev. **D66**, 075011 (2002).